Dilithium phthalocyanine - A Single Ion Transport Interfacial layer for Solid-State Lithium Batteries

*Chesta‡, Bindu K‡, S Sampath**

Department of Inorganic and Physical Chemistry, Indian Institute of Science, Bangalore-560012, India

KEYWORDS: All-solid-state-battery, LLZTO, dilithium phthalocyanine, interlayer, interfacial modification

ABSTRACT: All-solid-state batteries possess several advantages including high safety, flexibility to use high-capacity metal anodes and are projected to be the next generation energy storage devices. Garnet-type cubic $Li_7La_3Zr_2O_{12}$ (LLZO) solid electrolyte is of particular interest due to its high ionic conductivity under ambient conditions and compatibility with Li metal. However, large electrode/electrolyte interfacial resistance constraints their development. Herein, the use of a highly lithium ion conducting dilithium phthalocyanine (Li_2Pc) as an interlayer is proposed to effectively suppress the high impedance at the interface thus improving the electrode-electrolyte contact. Fast Li^+ mobility and high dielectric constant of dilithium phthalocyanine enhance the kinetics of Li^+ transport across the interface. A significant reduction in overpotential and very stable stripping/plating cycling are observed in lithium symmetric cells upon introducing Li_2Pc interlayer as compared to the use of bare tantalum doped lithium lanthanum zirconium oxide

(LLZTO) electrolyte. Cells comprising interlayer-modified Li|LLZTO|$LiFePO_4$ show high capacity with excellent cycling and rate capability. The performance of full cells using lithiated graphite and lithium titanate anodes has also been evaluated. This study presents a promising application of garnet electrolytes towards the advancement of solid-state lithium batteries.

1. Introduction

All-solid-state batteries (ASSB) are considered as suitable candidates for the next-generation energy storage devices. Despite several advantages in terms of safety, thermal/chemical stability and wide electrochemical stability window as compared to conventional liquid electrolytes, there are several challenges that hinder the development of these devices. One of the important issues is the high interfacial resistance between solid electrolyte and electrodes as the contacts are generally ineffective due to non-conformal morphologies and inefficient wettability. The uneven solid-solid interfaces limit ion migration and enhance the Li-dendrite formation on anodes.[1-3] The interfacial issues influence and limit the overall performance of the solid-state Li-ion battery. A space charge layer (SLC) is formed at the interface by the redistribution of mobile carriers upon contact of two phases with different chemical potentials.[4, 5] There are arguments put forward about the interfacial resistance and space charge effect on Li^+ transport but there is no clear experimental evidence yet, demonstrating the consequences of SCL in reducing interfacial resistance.[6-8] Usually, SCL is formed at the interface of an electrolyte and cathode, leading to the formation of lithium enriched state at the cathode side and lithium depleted state at the electrolyte side. This highly resistive lithium-depleted layer becomes a bottleneck for lithium-ion transport, particularly due to lack of charge carriers. It has been suggested that cathode interpose buffering layers (CIBLs) with strong lithium-ion attraction and high lithium-ion conduction, can hinder the formation of SCL.[6, 8, 9] In addition, interlayers with high permittivity can reduce the thickness of

SCL and in turn increase the kinetics of Li transport across electrode-electrolyte interface. In this direction, an interfacial layer with the possibility of Li single ion conduction having a high dielectric constant is a suitable candidate for all solid-state Li ion batteries (ASSB).[10]

The present study introduces the use of a macrocycle based on phthalocyanine as an interfacial layer for all solid-state Li ion battery. Phthalocyanines comprise a class of organic molecules with exceptionally high thermal and chemical stability.[11] They consist of conjugated 18 π electron ring system comprising of 4 isoindole groups with N atoms which form two coordination and two covalent bonds with the centre metal atom.[12] The electronic conductivity of dilithium phthalocyanine (Li_2Pc) originates from the overlap of π-π orbitals of the adjacent phthalocyanine (MPc) molecules. Metal phthalocyanines have been used as additives to improve Li ion transference and control dendritic growth in liquid-based Li rechargeable batteries. For instance, Li et. al. demonstrated the use of dilithium phthalocyanine as an electrolyte additive in Li-TFSI ionic liquid electrolyte to modify the ion solvation. The strong dipole-dipole interactions between Li_2Pc and polar solvent of the liquid electrolyte results in increased anion solvation. This reduces the anion mobility and in turn improves Li transference by increasing the Li salt dissociation. The authors show the high charge/discharge stability of the Li-S full cells accomplished by suppression of dendrite formation in presence of Li_2Pc in the electrolyte.[13] Similarly, use of cobalt phthalocyanine (CoPc) as an electrolyte additive results in the formation of a layer on Li metal anode resulting in uniform deposition of Li by decreasing the influence of space charge effect on Li deposition.[14] Modification of separator using Fe tetraamino-phthalocyanine helps in trapping lithium polysulfides resulting in the improvement of performance of Li-S batteries.[15] Depending upon the central metal atom and its valency, metal phthalocyanines exhibit different properties including catalytic activity, photoactivity, chemical and thermal stability. This results in their use

in a wide number of applications such as in coloration industry, catalysis, fuel cells, gas sensing, photosensitization, solar cells, organic light emitting diodes (OLEDs), thin film transistors, lubricants, indicators etc.[12, 16, 17]

Herein, dilithium phthalocyanine (Li_2Pc) is introduced as an interlayer between the solid garnet electrolyte and the cathode in an all-solid-state Li-ion battery. It has also been shown that the transport of Li ions is assisted by the presence of continuous negative electrostatic potential field in an organized assembly of Li_2Pc.[18] It is a mixed electronic-ionic conductor and the extent of ionic conduction is reported to be larger than that of the electronic conduction.[19] Scanlon et al. have studied an electrochemical cell with Li foil as anode, Li_2Pc as the solid electrolyte and Li_2Pc/MnO_2 as a composite cathode to explore the ionic conductivity between solid electrolyte and cathode. In the present study, garnet type solid electrolyte, tantalum doped lithium lanthanum zirconium oxide (LLTZO), is chosen to demonstrate the usefulness of Li_2Pc as an interlayer, since the electrolyte shows favorable electrochemical characteristics such as high ionic conductivity, negligible electronic conductivity, excellent chemical stability, and wider electrochemical stability window.[20] The Li ion mobility present in Li_2Pc acts as a bridge to facilitate Li ion transport from the solid electrolyte to cathode and reduces the interfacial resistance at the solid-solid interface.

2. Experimental Details

2.1. Materials Used

Lithium (Li) foil, dilithium phthalocyanine, lithium carbonate (Li_2CO_3), zirconium oxide (ZrO), lanthanum oxide (La_2O_3), tantalum oxide (Ta_2O_5), lithium cobalt oxide ($LiCoO_2$) and lithium iron phosphate ($LiFePO_4$) were purchased from Sigma, USA. Iso-propyl alcohol was purchased from SD Fine Chemicals, India. Lithium bis(trifluoromethanesulfonyl)imide (LiTFSI) was obtained from Solvionic, France. N-methyl n-propyl piperidinium bis(trifluoromethesulfonyl)imide was

purchased from ionic liquid technologies (io-li-tec), Germany. The dilithium phthalocyanine obtained from Sigma was a mixture of α and β phases and used without any further purification.

2.2. Synthesis of cubic LLZTO ($Li_7La_3Zr_{1.75}Ta_{0.25}O_{12}$)

LLZTO was synthesized using a modified Sono-chemical synthesis. This method leads to the formation of pure cubic phase LLZTO at lower temperatures as compared to the procedures reported in the literature.[21-23] Sono-chemical synthesis involves the use of ultrasonic waves to form acoustic cavitation or bubbles which grow and collapse impulsively leading to a high temperature and pressure at localized points. The heating and cooling rates at these cavities (bubbles) are > 10^{10} Ks^{-1} with a high localized temperature of ~500 K and a high localized pressure of ~1000 bar. Even though the intensity of ultrasonic waves generated by ultrasonic baths is low, it is sufficient for the distribution and reaction between solid precursors in a liquid medium. [24, 25] In this work, laboratory ultrasonic cleaning bath was used as the ultrasonic source for the synthesis of LLZTO. Stoichiometric amounts of Li_2CO_3 (50% extra for Li loss), ZrO_2, La_2O_3 and Ta_2O_3 (Sigma, USA) were ground in a mortar and pestle in the presence of isopropyl alcohol (IPA) for about 1 h. The powder obtained was sonicated in isopropyl alcohol (IPA) for 4 h. The mixture was further dried and ground for 30 min. and subsequently sintered in an alumina crucible at 900 ˚C for 12 h. followed by grinding for 1 h. and sintering at 980 ˚C for 12 h. Further, the powder was further ground for 1 h. and sintered at 980 ˚C for 12 h. The heating rate for all the steps was kept constant at 2 ˚C/min. The as formed powder material was transferred immediately to a desiccator to avoid atmospheric contamination.

2.3. Electrochemical characterization of solid electrolyte

LLZTO pellets were obtained by pressing LLZTO powder at an applied pressure of 14 tons using a hydraulic press. The pellets were sintered at 800 ˚C for 6 h. Sintered pellets were transferred

to a glove box and polished using an emery sheet before use. Electrochemical characterization was carried out in a coin cell assembly with different cell configurations. Symmetric cells were assembled using Li foils on both sides of the LLZTO pellet. Asymmetric cells were assembled using Li foil on one side and silver (Ag) on the other side. Li-blocking symmetric cells were assembled using silver on both sides of the pellet. Electrochemical impedance spectroscopy (EIS) measurements were recorded at room temperature in a frequency range of 7 MHz to 100 mHz with an amplitude of 20 mV.

2.4. Fabrication of full cells and electrochemical characterizations

Cells of Li|LLZTO|LFP configuration were fabricated using Li foil as anode, $LiFePO_4$ as cathode and LLZTO pellet as the solid electrolyte inside a glove box with moisture content less than 1 ppm. $LiFePO_4$ electrodes were fabricated by coating a slurry of $LiFePO_4$, acetylene black and polyvinylidene fluoride (PVDF) in a mass ratio of 7:2:1 in N-methyl-2-pyrrolidone (NMP) on Al-foil and dried in a vacuum oven at 80 ˚C for 12 h.

The LiC_6|LLZTO|LFP full cells were fabricated using lithiated graphite (LiC_6) as anode and LFP as the cathode. Graphite electrodes were prepared by coating a mixture of carbon powder, super P and PVDF (8:1:1) in NMP on Cu-foil followed by drying at 80 ˚C overnight in a vacuum oven. Half cells are assembled using Li foil as anode, graphite as cathode and 1 M $LiPF_6$ in ethylene carbonate/dimethyl carbonate (EC/DMC = 1:1) as the electrolyte. Lithiation of graphite was carried out by discharging the cells to 0 V at a slow rate of 10 mA g^{-1}. The lithiated graphite electrodes were recovered, washed with EC/DMC solvent and dried before fabricating a full cell in the solid-state battery configuration.

The full cells with configuration, LTO|LLZTO|LFP were assembled using LTO as anode and LFP as cathode. $Li_4Ti_5O_{12}$ electrodes were prepared by coating a slurry of $Li_4Ti_5O_{12}$, acetylene

black and PVDF in a mass ratio of 7:2:1 in NMP on a Cu foil and drying in a vacuum oven at 80 °C for 12 h. The diameter of electrolyte pellet, anode and cathode is kept constant as 10 mm for all the cells fabricated in this study. The loading of active material for all the cathodes prepared lies within 1.0-1.2 mg/cm^2.

Interfacial layer modification was carried out by coating a thin layer of Li_2Pc mixed with an ionic liquid electrolyte (ILE) (50 mg in 100 μL ILE) on both sides of the electrolyte pellet. The interlayer is indicated as LPIL throughout this study. Ionic liquid electrolyte was prepared by adding 0.25 M lithium bis(trifluoromethane-sulfonyl)imide (LiTFSI) in n-methyl n-propyl piperidinium bis(trifluoromethesulfonyl)imide with constant stirring. The LiTFSI was dried under vacuum at 120 °C for 12 h. prior to use. All the procedures were carried out under an inert atmosphere. For control experiments, only 10 μL of the ILE was added at both anode/electrolyte and cathode/electrolyte interfaces and used. Full cells without any interlayer were assembled for comparative studies. Galvanostatic charge-discharge studies were carried out using a Biologic VSP 300 electrochemical workstation. All the battery studies have been performed at room temperature.

2.5. Diffraction and spectroscopic characterizations

Powder X-ray diffraction (PANalytical) was used to characterize the powder and pellets. A Raman spectrometer (LabRAM HR, Horiba Jobin Yvon) equipped with 50XLWD objective, and a laser wavelength of 514 nm was used to obtain the Raman spectrum. Fourier transform infrared (FTIR) spectrum was recorded using a Perkin Elmer FTIR spectrometer. Scanning electron microscopy (SEM) images were obtained using a Carl Zeiss Ultra 55 microscope. X-ray photoelectron spectroscopic measurements were carried out using Thermo Scientific K-Alpha spectrometer with Al Kα radiation. A vacuum transfer module was used to load the Li anode,

electrolyte pellet and $LiFePO_4$ cathode samples inside the glove box. A pass energy of 50 eV and a spot size of 200 μm was used to record high-resolution spectra. A step size of 0.1 eV was used for all the measurements.

3. Results and discussion

3.1. Structure, composition, and electrochemical properties of LLZTO

The garnet LLZTO crystallizes in two polymorphs namely, tetragonal, and cubic structures with space groups $I4_1/acd$ and Ia-3d respectively. Both tetragonal and cubic structures have 8 formula units in a unit cell and the ionic conductivity depends on the occupancy of Li in the lattice sites. Doping of Ta in LLZO favors the stabilization of cubic phase at lower temperature by changing the site preference of lithium ion from octahedral to tetrahedral.[26] The conventional solid-state synthesis of garnet-type solid electrolytes requires multiple sintering steps at temperatures above 1050 ˚C with each sintering step comprising of 24 h. or higher (Table S1). The present study proposes the use of ultrasonic energy to reduce the sintering temperature and the time required to obtain pure cubic phase of LLZTO. The introduction of ultrasonication facilitates the formation of cubic LLZO at a relatively lower temperature of 980 ˚C. Furthermore, the lower of sintering temperature reduces the extent of Li loss during sintering.[27, 28]

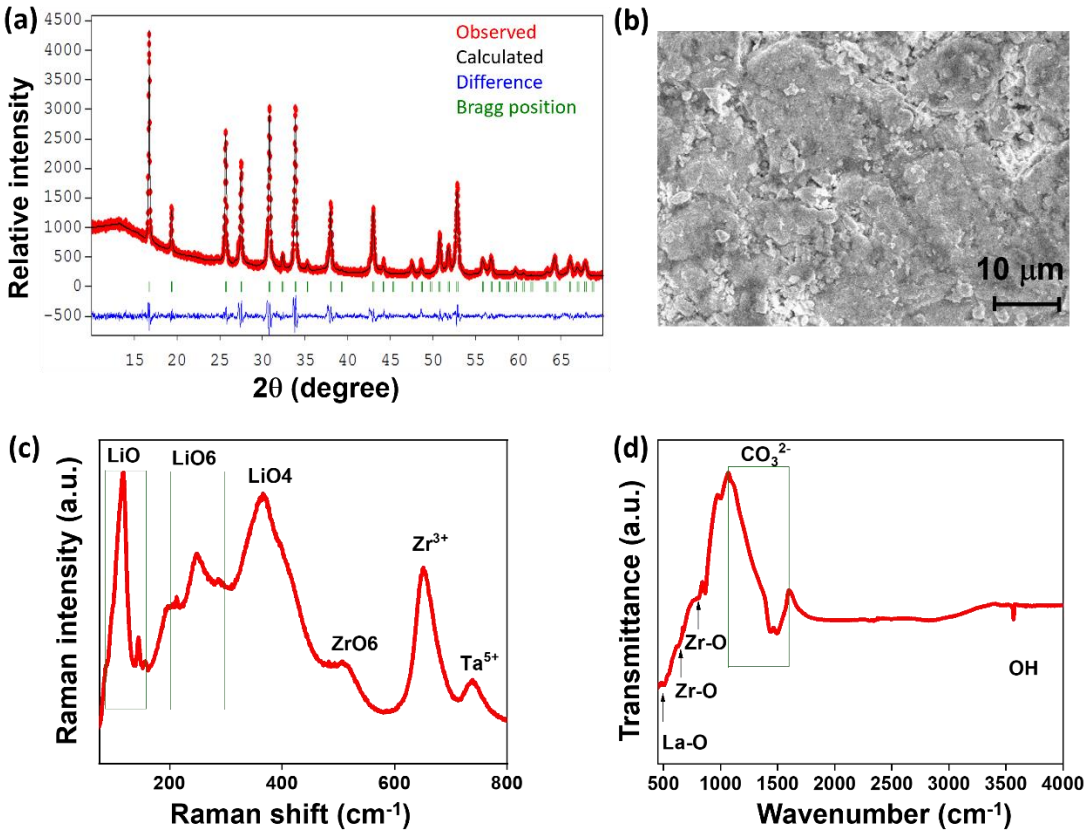

Figure 1. (a) Diffraction pattern of the as-synthesized LLZTO powder along with the Rietveld refined pattern, (b) SEM image of LLZTO pellet, (c) Raman spectrum and (d) FTIR spectrum of the LLZTO powder.

The XRD pattern of the as-synthesized LLZTO powder is shown in Figure 1a and it indicates the formation of pure cubic phase without any impurity phase and well matches with the corresponding standard powder pattern (45-109). The Rietveld refined XRD pattern clearly identifies a pure, cubic, single-phase compound, $Li_7La_3Zr_{1.75}Ta_{0.25}O_{12}$. Figure S1 shows the XRD of LLZTO pellets sintered at different temperatures. It is observed that cubic phase is retained at all temperatures. However, a peak corresponding to a pyrochlore phase, $La_2Zr_2O_7$ (marked by ♦) emerges at sintering temperatures at and above 900 ˚C and is likely to be due to lithium loss at these temperatures. Hence, the present preparation method using a sonication step helps in not

only optimizing the sintering temperature at 800 ˚C but also avoids any impurity phase due to lithium loss. SEM image of the LLZTO pellet shows that they are compact, and the grain boundaries are well-connected on sintering the pellets at 800 ˚C (Figure 1b). At 800 ˚C, highly dense pellets are obtained without observable pores.

The Raman spectrum of LLZTO shown in Figure 1c indicates the presence of a pure cubic phase. Bands in the region 300-550 cm^{-1} are due to the vibrational bending modes of LiO_4 tetragonal unit. The ones above 550 cm^{-1} may be assigned to the stretching mode of ZrO_6 octahedral unit. Below 300 cm^{-1}, vibrational stretches of LiO_6 octahedral unit are present. The bands at 737 cm^{-1} and 651 cm^{-1} in pure LLZTO correspond to Ta^{5+} and Zr^{3+} respectively[29] and the narrow bands in the low frequency region, below 200 cm^{-1}, correspond to Li-O vibrational bending modes.[30] Figure 1d shows the FTIR spectrum of LLZTO and the observed bands at 630 and 841 cm^{-1} correspond to Zr-O vibrations while the one at 482 cm^{-1} is assigned to La-O vibration. The signatures in the region from 1000 to 1650 cm^{-1} are due to CO_3^{2-} and the O-H stretch is observed above 3500 cm^{-1}.[30] The source of CO_3^{2-} in the sample may be from the Li_2CO_3 precursor or the formation of Li_2CO_3 on the pellet surface on exposure to air during the measurements.

The ionic and electronic conductivities of LLZTO pellets have been determined using impedance spectroscopy and chronoamperometry (CA) techniques. The Nyquist plot of Ag|LLZTO|Ag cell is shown the Figure 2a. The LLZTO with blocking electrodes shows a depressed semicircle at high frequency region along with a diffusion spike at low frequency region. The semicircle at higher frequency can be attributed to the total impedance of LLZTO pellet which includes contribution from the bulk and grain boundaries whereas the diffusion spike at the lower frequency can be assigned to the Li^+ ion blocking behavior at the interface of electrode and solid electrolyte.

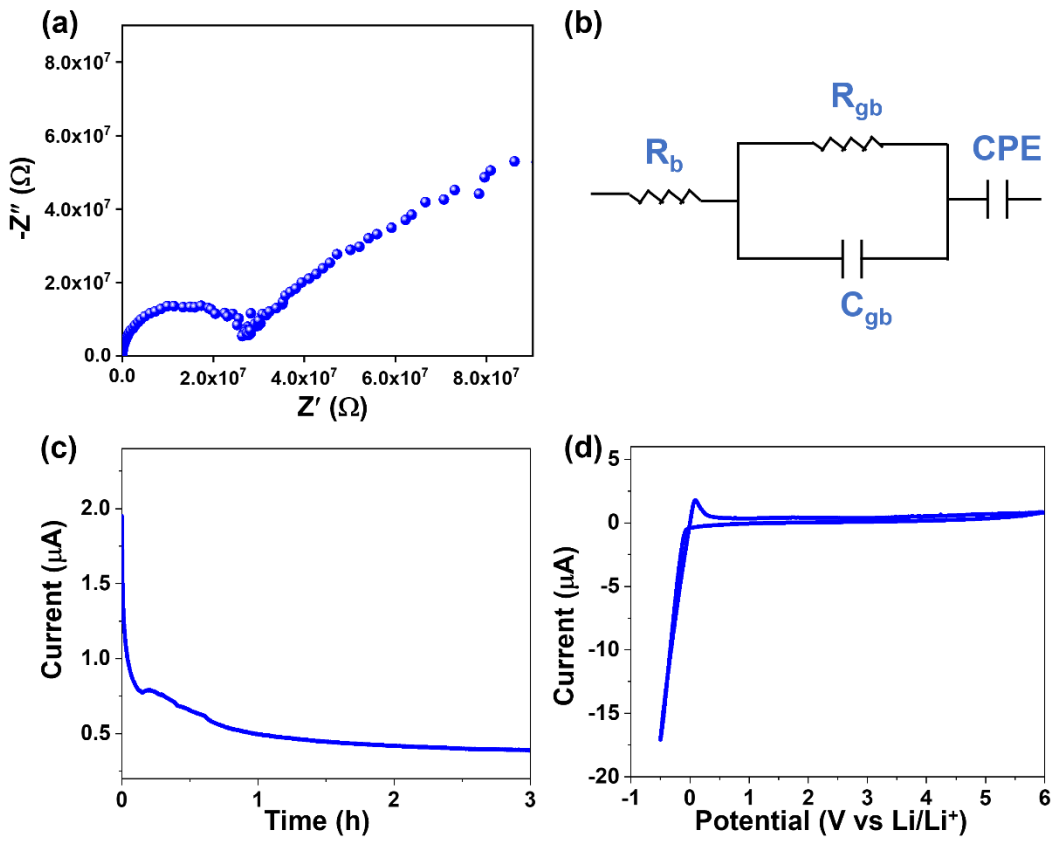

Figure 2. (a) Nyquist plot, (b) Equivalent circuit, (c) Chronoamperometry data for LLZTO in Ag|LLZTO|Ag configuration, and (d) Cyclic voltammetry of the cell, using Ag|LLZTO|Li configuration.

The Nyquist plot can be fitted to an equivalent circuit model (R_b) (R_{gb}-C_{gb}) (CPE) as shown in Figure 2b. Here, R_b is bulk resistance, R_{gb} is grain boundary resistance, CPE_{gb} and CPE are constant phase elements for grain boundary capacitance and the diffusion capacitance at the electrode/electrolyte interface respectively. The values of R_b, R_{gb} and C_{gb} are 29.4 Ω, 28 MΩ, and 42 pF, respectively. The intercept of semicircle to the x-axis at high frequency region is considered as the bulk resistance which is the resistance of the electrolyte. This resistance can be used to estimate the ionic conductivity of the electrolyte using the relation, $\sigma_t = \frac{d}{AR_i}$, where σ_t is the ionic conductivity of the solid electrolyte, d is the thickness of the pellet, A is the area of the pellet and

R_i is the ionic resistance of the electrolyte. The values of R_b, R_{gb} and C_{gb} are 29.4 Ω, 28 MΩ, and 42 pF, respectively.

The total Li-ionic conductivity of LLZTO pellets is found to be 3.31×10^{-4} S cm^{-1} and the electronic conductivity (Figure 2c) is estimated to be 1.3×10^{-8} S cm^{-1}. These values are similar to the ones reported for LLZTO synthesized at high temperatures.[21-23] EIS was also recorded for pellets sintered at different temperatures. The ionic conductivity calculated from Nyquist plots shown in Figure S2 depict the values of 1.3×10^{-4}, 0.07×10^{-4}, and 0.15×10^{-4} S cm^{-1} at the sintering temperatures of 700 °C, 900 °C and 980 °C respectively. The stability window of LLZTO evaluated using cyclic voltammetry using an asymmetric cell of LLZTO pellet coated with silver and lithium on either side at a scan rate of 5 mVs^{-1} in the potential range of -0.5 V to 6 V is shown in Figure 2d. The representative redox current at around -0.1 V and peak at 0.09 V suggest Li plating/stripping processes respectively. No other significant redox current is observed in the entire voltage range, suggesting a wide electrochemical stability window of LLZTO up to 6 V versus metallic Li.[31]

3.2. Electrochemical properties of Li_2Pc interlayer modified solid-state batteries

Proper interfacial contact between LLZTO electrolyte and electrodes is crucial for enhanced ion transport and even current distribution at the interface. In the present study, Li_2Pc is used as an interfacial layer. Li_2Pc is different from other metal phthalocyanines in terms of number of metal ions per phthalocyanine molecule and the position of the metal ion. While most metal phthalocyanines are planar and contain one divalent metal ion at the center of the phthalocyanine ring, Li_2Pc contains 2 Li, one above and one below the plane of phthalocyanine ring. Ab initio calculations reveal that dilithium phthalocyanine in its crystalline form, favors the formation of molecular assembly due to the presence of attractive forces between Li_2Pc molecules. It has been

calculated that the distance between two Li ions increases from 1.99 Å in a single Li_2Pc molecule to 2.67 Å in the self-assembled structure.[32] This may be due to weakening of Li-N bond and results in ionic conductivity through a Li ion conducting channel. The presence of attractive forces between Li ion and negatively charged nitrogen atoms of adjacent C in Li_2Pc helps in this direction.

Figure 3a shows the Nyquist plots for Li|LLZTO|Li symmetric cells with LLZTO electrolyte. The symmetric cell without interlayer exhibits single semicircle with high impedance. This indicates that the bulk resistance and interfacial resistance of the cell are large which makes it difficult to separate them. On the other hand, symmetric cells with interfacial modifications present two semicircles at the high frequency region along with an extended tail at the low frequency region. The Nyquist plots can be fitted with Huggin's model.[33] The higher frequency region of the initial semicircle (R1+(R2||Q1)) indicates the total resistance of the pellet which includes the ionic resistance part from the grains and grain boundary regions of the pellet. The second semicircle along with the extended tail at the lower frequency ((R3||Q2) +Q3) indicates the interfacial resistance along with the impedance caused by electric relaxations respectively. The half of the size of the second semicircle is considered to be the Area Specific resistance (ASR) of the interface.[34] It is clearly observed that the Li_2Pc interlayer significantly reduces the total impedance from 280 MΩ cm^2 for the bare interface to 1084 Ω cm^2 in the presence of Li_2Pc interlayer. In comparison, interface with pure ionic liquid has a total impedance of 6912 Ω cm^2. The interfacial ASR has been found to reduce from 95 MΩ cm^2 for the bare interface to 1220 Ω cm^2 for the ionic liquid modified cells which further reduces to 190 Ω cm^2 for Li_2Pc modified interface cells. A comparison of ASR with different interfacial modifications is shown in Figure S3.

To understand the Li-ion transport resistance associated with Li-ion movement from solid electrolyte to cathode (LFP), impedance measurements have been carried out for symmetric LFP

electrode cells (LFP|LLZTO|LFP) with different interface modifications. Figure 3b shows the corresponding Nyquist plots and the data can be fitted with the (R1+(R2||Q2)+Q3) circuit where R1 represents the bulk resistance of the pellet, R2 indicates the interfacial resistance between the electrolyte and the $LiFePO_4$ cathode and Q3 is the impedance caused by electric relaxation at the interface.

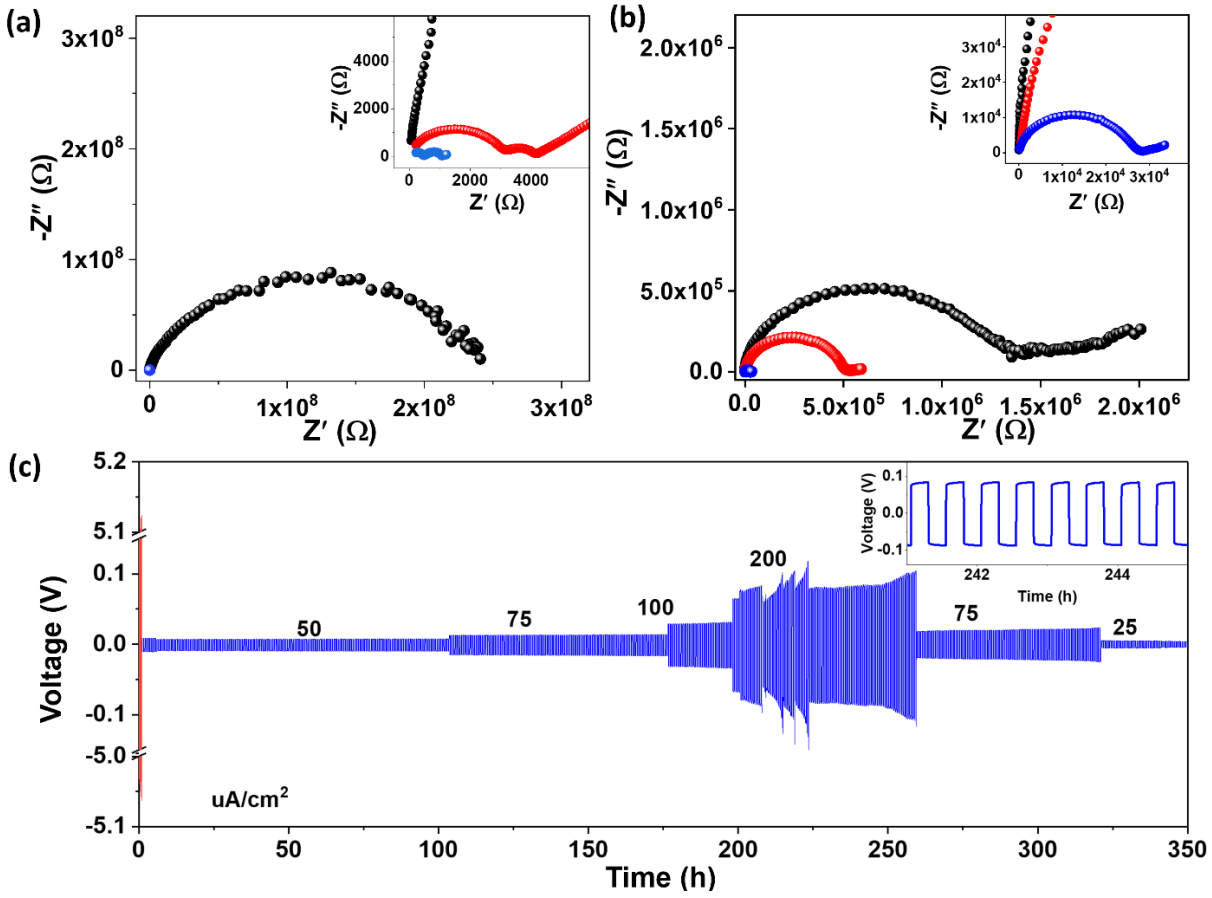

Figure 3. Nyquist plots for (a) Li|LLZTO|Li symmetric cell and (b) LFP|LLZTO|LFP symmetric cell and (c) Galvanostatic cycling performance of Li|LLZTO|Li symmetric cell with different interlayers, black - no interlayer (Figure 3a, b), red - ionic liquid interlayer and blue - LPIL interlayer at the interfaces.

The charge transfer resistance between the cathode and the LLZTO solid electrolyte without any interlayer is quite high and is of the order of 10^6 Ω which is due to insufficient mechanical contact between the rigid LLZTO electrolyte and the cathode. The poor contact forms a dead area where cathode particles are completely isolated from the LLZTO electrolyte. Neither electron nor Li^+-ions can be transported in these areas due to lack of percolation path and this leads to the localized non-uniform distribution of current and strain.[35] In addition, the formation a space-charge layer is also favoured.[36-38]

The ionic liquid alone as an interlayer reduces the charge transfer resistance by one order of magnitude (10^5 Ω). On the other hand, the presence of LPIL interlayer greatly improves the Li ion mobility between LLZTO and $LiFePO_4$ and further reduces the interfacial resistance to 10^4 Ω. This suggests that the presence of Li ion conducting channels in Li_2Pc improves the kinetics of Li ion transfer at the interface. The dielectric constant (Figure 4) measurements further confirm that there is a significant decrease in the space charge layer, which leads to a uniform distribution of charges at the interface.[39]

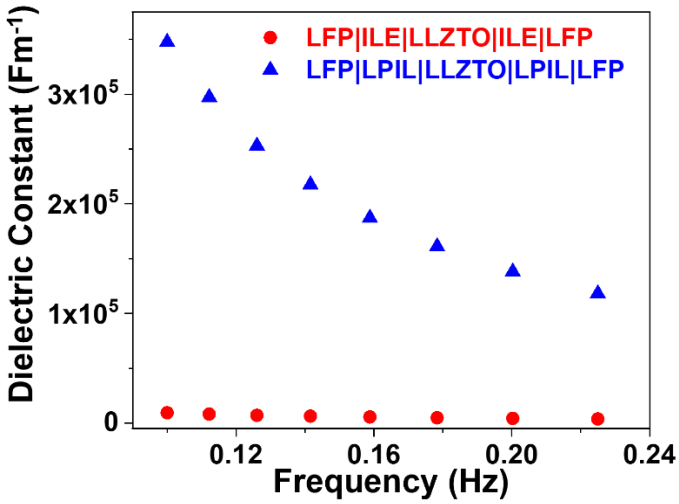

Figure 4. Dielectric constant values of LFP|LLZTO|LFP cathode symmetric cell with different interlayers, red - ionic liquid interlayer and blue – LPIL interlayer at the interfaces.

Galvanostatic charge-discharge behaviour of Li|LLZTO|Li symmetric cells with and without interlayers are carried out to understand the cycling stability. The cell without interlayer does not exhibit enough cycling ability due to high interfacial resistance between the electrolyte and Li-metal.[40-42] The stripping/ plating behaviour of the cells with ionic liquid alone and with LPIL interlayers are shown in Figure 3c. Comparison of charge-discharge cycles for the cells with LPIL interlayer at 50 $\mu A/cm^2$ shows that the interface modified with ionic liquid alone shows high polarization overpotential. On the contrary, Li_2Pc modified cell shows a low polarization overpotential and the interface is quite stable for long-term stripping/plating at different current densities of 50 and 75, 100 and 200 $\mu A/cm^2$. These results conclude that there is a formation of stable interface on introduction of Li_2Pc at the junction of electrode and the electrolyte. Research on the use of metal phthalocyanines in improving the performance of batteries has recently gained attention and there are very limited studies exploring the use of phthalocyanines in batteries containing liquid electrolytes. For instance, cobalt phthalocyanine (CoPc) has been reported to form a protective layer on the Li anode surface by complexing with Li ions when used as an electrolyte additive along with the conventional ester-based liquid electrolyte (1 M lithium hexafluorophosphate in a mixture of ethylene carbonate (EC)/diethyl carbonate (DEC)). The presence of CoPc in the electrolyte results in uniform Li deposition and stable interphase formation which leads to reduced dendritic growth and long-term cycling stability of Li|Li symmetric cell for upto 700 h.[14] On the other hand, the present study depicts the role of Li_2Pc in stabilizing the interfaces in an all-solid-state battery.

3.3. Performance of Li_2Pc interlayer modified Li metal solid-state batteries

To evaluate the cell performance with stable interfacial layers, the characteristics are measured using Li metal anode, $LiFePO_4$ cathode and LPIL interlayer at the electrode/electrolyte interface

as depicted in the schematics given in Figure 5a. Figure 5b shows the charge-discharge curves of Li|LLZTO|LFP with LPIL interlayer. It is observed that the initial discharge capacity of the cell is 68 mAh g^{-1} at a current rate of 5 mA g^{-1}. The specific capacity increases to 80 mAh g^{-1} in the second cycle and is maintained till 6th cycle after which the cell delivers an average capacity of 72 mAh g^{-1}. In comparison, the cell with ionic liquid interlayer alone shows a quite low capacity (Figure S4). This suggests that the presence of LPIL interlayer greatly stabilizes the solid electrolyte interlayer and cathode-electrolyte interlayer formation between Li-metal/LLZTO and LFP/LLZTO respectively. The present interlayer holds the advantage of high Li-ion mobility due to reduction in the solvation around Li ions induced by the presence of Li_2Pc in the Li-TFSI ionic liquid electrolyte. The dilithium phthalocyanine in Li-TFSI ionic liquid electrolyte reduces the solvation around the Li-ions and increase the Li-ion mobility.[13]

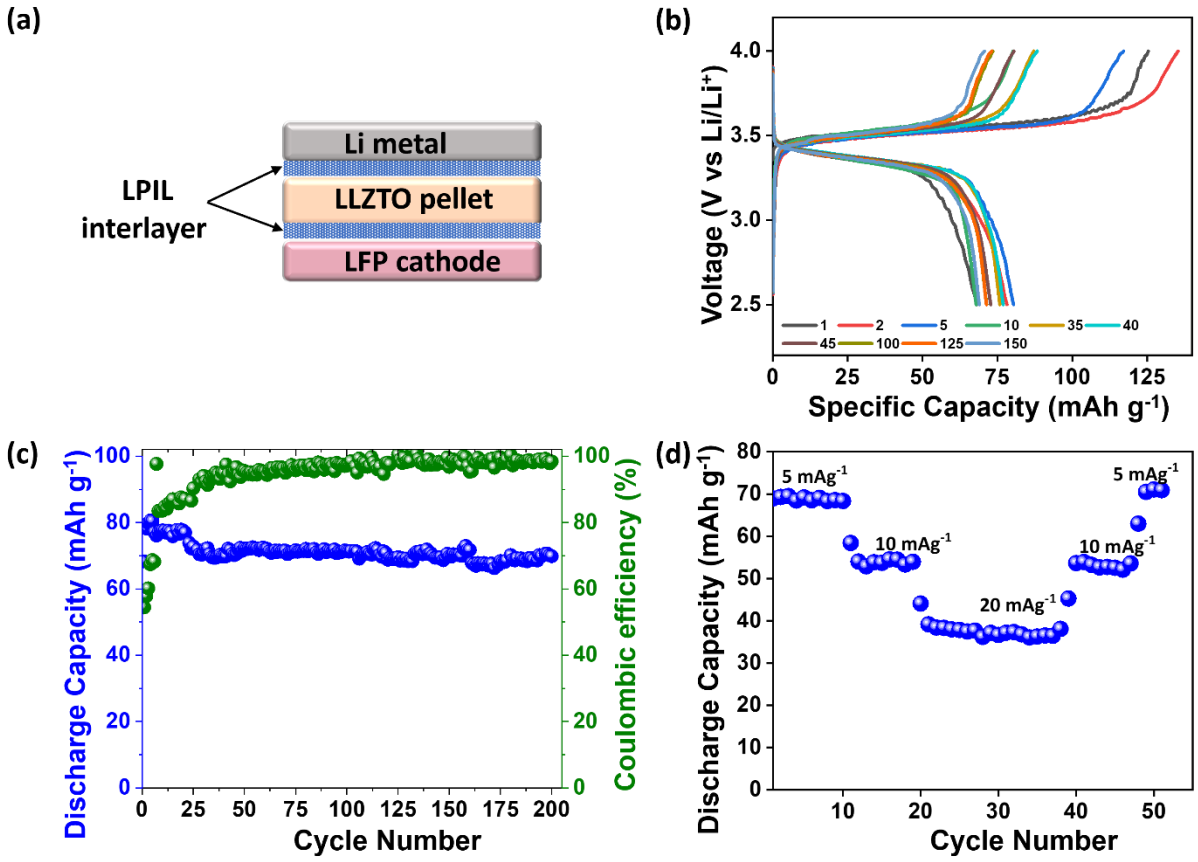

Figure 5. (a) Schematic illustration of the Li|LPIL|LLZTO|LPIL|LFP cell, (b) Voltage profile, (c) Long-term cycling stability of the cell at a current density of 5 mA g^{-1} and (d) Rate performance of the interlayer modified cells at different current densities.

The solid-state battery exhibits excellent charge/discharge cycling stability for 200 cycles with a capacity retention of 90 % and coulombic efficiencies of 95-100 % as shown in Figure 5c. Figure 5d shows the rate capability of the cell. The cell shows a capacity of ~70 mAh g^{-1}, 54 mAh g^{-1} and 40 mAh g^{-1} at an applied current density of 5, 10 and 20 mA g^{-1} respectively. Another cell modified with a thin layer of molten Li on LLZTO pellet as the anode, along with $LiFePO_4$ cathode and LPIL interlayer at the cathode/electrolyte interface is studied. The cell is cycled at different current densities and the performance is found to be similar to that of the cell with LPIL interlayer at both the interfaces (Figure S5).

3.4. Post-cycling studies of the Li_2Pc interlayer

To further understand the interfacial behaviour, x-ray photoelectron spectroscopy is carried out on the surface of $LiFePO_4$ cathode and Li metal anode after 100 cycles of charge-discharge using LPIL interlayer at a current density of 5 mA g^{-1} (Figure S6-S9). A detailed analysis of the XPS data is summarized in Table S2 and Table S3. The Li anode of the cell with the ionic liquid interlayer turns black and brittle while the one with the LPIL interface is stable with the colour of the Li_2Pc as evident from Figure 6.

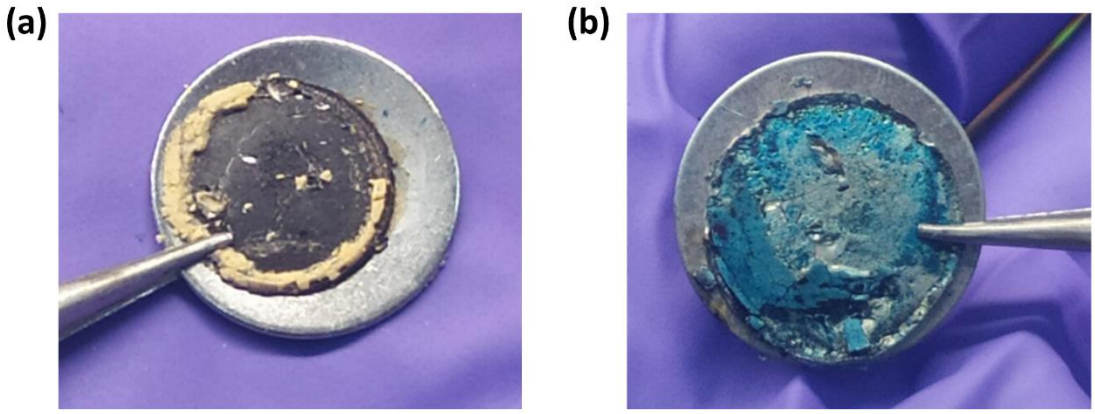

Figure 6. Digital images of Li anodes after 100 cycles of charge-discharge at 5 mA g^{-1} current density for (a) Li|ILE|LLZTO|ILE|LFP and (b) Li|LPIL|LLZTO|LPIL|LFP cells.

In the Li 1s high resolution XPS spectrum, a peak at 54.77 eV indicates that the black colour is due to the formation of lithium-nitrogen compounds during cycling.[43, 44] Along with this, formation of Li_2CO_3 is confirmed from the peaks present at 289.75 eV, 55.15 eV and 532.01 eV corresponding to the C 1s, Li 1s and O 1s regions respectively.[45, 46] The presence of Li_2CO_3 can hinder the Li-exchange between the electrolyte and the electrode which negatively affects the performance of the cell.[33,34] On the other hand, Li anode in the cell with LPIL interlayer is intact and the formation of lithium fluoride, LiF, on the Li-metal surface is evident from the peaks at 684.4 eV peak in F 1s and 56.2 eV in Li 1s regions [47]. The peak at 54.65 eV in the Li 1s region indicates the formation of LiOH.[48, 49] The formation of LiF formed during the cycling by the interaction of Li_2Pc and LiTFSI assists in repairing the solid electrolyte interface (SEI) and helps to protect the electrode surface avoiding side reactions between electrolyte and electrode.[50, 51] The XPS studies reveal that the addition of Li_2Pc substantially prevents the decomposition of ionic liquid on cycling. The peaks at 55.55 eV in Li 1s, 288.8 eV in C 1s and 532.11 eV in O 1s regions obtained for the cathode of the cell with ionic liquid interlayer confirms the presence of Li_2CO_3.

On the contrary, Li_2CO_3 is absent on the cathode for the cell with LPIL interlayer. Apart from this observation, LiF is formed on the cathode surface of the former cell while it is absent in the latter. These results suggest that the LPIL interlayer successfully stabilizes the interface by suppressing the formation of Li_2CO_3 and promoting the formation of LiF.

The LLZTO solid electrolyte with LPIL interlayer is integrated in a complete solid-state full cell with LiC_6 anode and LFP cathode and preliminary studies have been carried out. The charge-discharge curves of the LPIL interlayer modified LiC_6|LLZTO|LFP at a current density of 5 mA g^{-1} is shown in Figure S10a. The cell displays an initial discharge specific capacity of 32 mAh g^{-1} and is retained at a value of 38 mAh g^{-1} after 40 cycles. Similarly, full cell performance has been evaluated using LTO anode as shown in Figure S10b. An initial discharge capacity of 41 mAh g^{-1} is achieved at a current density of 5 mA g^{-1} and is retained at 37 mAh g^{-1} after 80 cycles. In comparison, the ionic liquid modified full cell using LTO anode and LFP cathode shows a capacity of 10 mAh g^{-1} at the same rate (Figure S11). As expected, the full cell with Li-metal anode delivers higher capacity than the full cells with LiC_6 and LTO anodes due to high lithium inventory in the case of lithium metal anode as compared to the LiC_6 and LTO anodes.[52, 53]The full cells can be further optimized to obtain better performance.

4. Summary

The incorporation of LPIL interlayer has been studied to successfully address the poor interface between electrodes and garnet-type LLZTO solid electrolyte. The LPIL interlayer significantly reduces the area specific resistance between Li-metal and LLZTO electrolyte from 95 MΩ cm^2 to 190 Ω cm^2. Also, the interfacial resistance between the cathode and LLZTO reduces from 5.4 MΩ cm^2 to 10 kΩ cm^2. Li_2Pc effectively stabilizes the interface and shows a long-term cycling stability with low overpotential for symmetric cells. Li_2Pc is found to successfully improve the electrode /

garnet-type solid electrolyte interface, thereby enhancing the performance of the cells both in Li-metal anode and Li-compound anode cells. This work provides an insight into the role of macrocycles as efficient interlayers that are cost effective and scalable.

Associated content

The following files are available free of charge.

Supporting Information (PDF)

Corresponding Author

*Sampath S, Professor, Department of Inorganic and Physical Chemistry, Indian Institute of Science, Bangalore-560012. ssampath2010@gmail.com.

Authors

Chesta, Department of Inorganic and Physical Chemistry, Indian Institute of Science, Bangalore-560012. chesta16447@iisc.ac.in.

Bindu K, Department of Inorganic and Physical Chemistry, Indian Institute of Science, Bangalore-560012. bindukphy@gmail.com.

Author Contributions

Chesta‡ - Experiments, analysis and manuscript writing

Bindu K‡ - Experiments, analysis and manuscript writing

Sampath S – Supervision, manuscript correction

‡Authors Chesta and Bindu K have equal contribution in the manuscript.

ACKNOWLEDGMENT

Dr. Bindu K and Ms. Chesta would like to thank UGC and CSIR for D S Kothari post-doctoral fellowship and Junior/Senior Research fellowship respectively. SS thanks IGSTC, New Delhi for providing research funds.

REFERENCES

(1) Kobayashi, S.; Arguelles, E. F.; Shirasawa, T.; Kasamatsu, S.; Shimizu, K.; Nishio, K.; Watanabe, Y.; Kubota, Y.; Shimizu, R.; Watanabe, S.; et al. Drastic Reduction of the Solid Electrolyte–Electrode Interface Resistance via Annealing in Battery Form. *ACS Applied Materials & Interfaces* **2022**, *14* (2), 2703-2710. DOI: 10.1021/acsami.1c17945.

(2) Xu, P.; Rheinheimer, W.; Mishra, A.; Shuvo, S. N.; Qi, Z.; Wang, H.; Dongare, A. M.; Stanciu, L. A. Origin of High Interfacial Resistance in Solid-State Batteries: LLTO/LCO Half-Cells**. *ChemElectroChem* **2021**, *8* (10), 1847-1857. DOI: https://doi.org/10.1002/celc.202100189.

(3) Lou, S.; Liu, Q.; Zhang, F.; Liu, Q.; Yu, Z.; Mu, T.; Zhao, Y.; Borovilas, J.; Chen, Y.; Ge, M.; et al. Insights into interfacial effect and local lithium-ion transport in polycrystalline cathodes of solid-state batteries. *Nature Communications* **2020**, *11* (1), 5700. DOI: 10.1038/s41467-020-19528-9.

(4) Wang, L.; Xie, R.; Chen, B.; Yu, X.; Ma, J.; Li, C.; Hu, Z.; Sun, X.; Xu, C.; Dong, S.; et al. In-situ visualization of the space-charge-layer effect on interfacial lithium-ion transport in all-solid-state batteries. *Nature Communications* **2020**, *11* (1), 5889. DOI: 10.1038/s41467-020-19726-5.

(5) Yang, H.; Mu, D.; Wu, B.; Bi, J.; Zhang, L.; Rao, S. Improving cathode/Li6.4La3Zr1.4Ta0.6O12 electrolyte interface with a hybrid PVDF-HFP-based buffer layer for solid lithium battery. *Journal of Materials Science* **2020**, *55* (25), 11451-11461. DOI: 10.1007/s10853-020-04701-8.

(6) Cheng, Z.; Liu, M.; Ganapathy, S.; Li, C.; Li, Z.; Zhang, X.; He, P.; Zhou, H.; Wagemaker, M. Revealing the Impact of Space-Charge Layers on the Li-Ion Transport in All-Solid-State Batteries. *Joule* **2020**, *4* (6), 1311-1323. DOI: https://doi.org/10.1016/j.joule.2020.04.002.

(7) de Klerk, N. J. J.; Wagemaker, M. Space-Charge Layers in All-Solid-State Batteries; Important or Negligible? *ACS Applied Energy Materials* **2018**, *1* (10), 5609-5618. DOI: 10.1021/acsaem.8b01141.

(8) Swift, M. W.; Qi, Y. First-Principles Prediction of Potentials and Space-Charge Layers in All-Solid-State Batteries. *Physical Review Letters* **2019**, *122* (16), 167701. DOI: 10.1103/PhysRevLett.122.167701.

(9) Chen, C.; Guo, X. Space Charge Layer Effect in Solid State Ion Conductors and Lithium Batteries: Principle and Perspective. *Acta chimica Slovenica* **2016**, *63* (3), 489-495. DOI: 10.17344/acsi.2016.2286 From NLM.

(10) Ohno, T.; Shimizu, N.; Ohkubo, K.; Hanashima, T.; Yamawaki, K.; Sasaki, S. Site preference of valence ions in Fe1+xCo2-xO4 (0 <= x <= 1). *Acta Crystallographica Section A* **2005**, *61* (a1), c401. DOI: doi:10.1107/S0108767305083005.

(11) de la Torre, G.; Bottari, G.; Hahn, U.; Torres, T. Functional Phthalocyanines: Synthesis, Nanostructuration, and Electro-Optical Applications. In *Functional Phthalocyanine Molecular Materials*, Jiang, J. Ed.; Springer Berlin Heidelberg, 2010; pp 1-44.

(12) Cranston, R. R.; Lessard, B. H. Metal phthalocyanines: thin-film formation, microstructure, and physical properties. *RSC Advances* **2021**, *11* (35), 21716-21737, 10.1039/D1RA03853B. DOI: 10.1039/D1RA03853B.

(13) Li, X.; Fu, Z.; Wang, J.; Zhao, X.; Zhang, Y.; Liu, W.; Cai, Q.; Hu, C. Dilithium phthalocyanine as electrolyte additive for the regulation of ion solvation and transport towards dendrite-free Li metal anodes. *Chemical Engineering Journal* **2022**, *450*, 138112. DOI: https://doi.org/10.1016/j.cej.2022.138112.

(14) Dai, H.; Dong, J.; Wu, M.; Hu, Q.; Wang, D.; Zuin, L.; Chen, N.; Lai, C.; Zhang, G.; Sun, S. Cobalt-Phthalocyanine-Derived Molecular Isolation Layer for Highly Stable Lithium Anode. *Angewandte Chemie International Edition* **2021**, *60* (36), 19852-19859. DOI: https://doi.org/10.1002/anie.202106027.

(15) Li, X.; Yang, X.; Ye, J.; Xia, G.; Fu, Z.; Hu, C. A trifunctional modified separator based on Fe tetraaminophthalocyanine@rGO for lithium-sulfur batteries. *Chemical Engineering Journal* **2021**, *405*, 126947. DOI: https://doi.org/10.1016/j.cej.2020.126947.

(16) Tomeček, D.; Piliai, L.; Hruška, M.; Fitl, P.; Gadenne, V.; Vorokhta, M.; Matolínová, I.; Vrňata, M. Study of Photoregeneration of Zinc Phthalocyanine Chemiresistor after Exposure to Nitrogen Dioxide. *Chemosensors* **2021**, *9* (9), 237.

(17) Grobosch, M.; Schmidt, C.; Kraus, R.; Knupfer, M. Electronic properties of transition metal phthalocyanines: The impact of the central metal atom (d5–d10). *Organic Electronics* **2010**, *11* (9), 1483-1488. DOI: https://doi.org/10.1016/j.orgel.2010.06.006.

(18) Scanlon, L. G.; Lucente, L. R.; Feld, W. A.; Sandi, G.; Balbuena, P. B.; Alonso, P. R.; Turner, A. Composite Cathode with Li[sub 2]Pc. *Journal of The Electrochemical Society* **2004**, *151* (9), A1338. DOI: 10.1149/1.1772780.

(19) Munichandraiah, N.; Sakthivel, K.; Scanlon, L. G. Analysis of Electrochemical Impedance of Dilithium Phthalocyanine. *Electrochemical and Solid-State Letters* **2005**, *8* (5), E45-E48. DOI: 10.1149/1.1872592.

(20) Wang, C.; Fu, K.; Kammampata, S. P.; McOwen, D. W.; Samson, A. J.; Zhang, L.; Hitz, G. T.; Nolan, A. M.; Wachsman, E. D.; Mo, Y.; et al. Garnet-Type Solid-State Electrolytes: Materials, Interfaces, and Batteries. *Chemical Reviews* **2020**, *120* (10), 4257-4300. DOI: 10.1021/acs.chemrev.9b00427.

(21) Buschmann, H.; Dölle, J.; Berendts, S.; Kuhn, A.; Bottke, P.; Wilkening, M.; Heitjans, P.; Senyshyn, A.; Ehrenberg, H.; Lotnyk, A.; et al. Structure and dynamics of the fast lithium ion conductor “Li7La3Zr2O12”. *Physical Chemistry Chemical Physics* **2011**, *13* (43), 19378-19392, 10.1039/C1CP22108F. DOI: 10.1039/C1CP22108F.

(22) Rangasamy, E.; Wolfenstine, J.; Sakamoto, J. The role of Al and Li concentration on the formation of cubic garnet solid electrolyte of nominal composition Li7La3Zr2O12. *Solid State Ionics* **2012**, *206*, 28-32. DOI: https://doi.org/10.1016/j.ssi.2011.10.022.

(23) Shin, B. R.; Nam, Y. J.; Oh, D. Y.; Kim, D. H.; Kim, J. W.; Jung, Y. S. Comparative Study of TiS2/Li-In All-Solid-State Lithium Batteries Using Glass-Ceramic Li3PS4 and Li10GeP2S12 Solid Electrolytes. *Electrochimica Acta* **2014**, *146*, 395-402. DOI: https://doi.org/10.1016/j.electacta.2014.08.139.

(24) Bang, J. H.; Suslick, K. S. Applications of Ultrasound to the Synthesis of Nanostructured Materials. *Advanced Materials* **2010**, *22* (10), 1039-1059. DOI: https://doi.org/10.1002/adma.200904093.

(25) Calderón-Jiménez, B.; Montoro Bustos, A. R.; Pereira Reyes, R.; Paniagua, S. A.; Vega-Baudrit, J. R. Novel pathway for the sonochemical synthesis of silver nanoparticles with near-spherical shape and high stability in aqueous media. *Scientific Reports* **2022**, *12* (1), 882. DOI: 10.1038/s41598-022-04921-9.

(26) Chen, F.; Li, J.; Huang, Z.; Yang, Y.; Shen, Q.; Zhang, L. Origin of the Phase Transition in Lithium Garnets. *The Journal of Physical Chemistry C* **2018**, *122* (4), 1963-1972. DOI: 10.1021/acs.jpcc.7b10911.

(27) Zhao, X.; Gao, J.; Khalid, B.; Zijian, Z.; Wen, X.; Geng, C.; Huang, Y.; Tian, G. Sintering analysis of garnet-type ceramic as oxide solid electrolytes for rapid Li+ migration. *Journal of the European Ceramic Society* **2022**, *42* (15), 7063-7071. DOI: https://doi.org/10.1016/j.jeurceramsoc.2022.08.053.

(28) Ihrig, M.; Mishra, T. P.; Scheld, W. S.; Häuschen, G.; Rheinheimer, W.; Bram, M.; Finsterbusch, M.; Guillon, O. Li7La3Zr2O12 solid electrolyte sintered by the ultrafast high-temperature method. *Journal of the European Ceramic Society* **2021**, *41* (12), 6075-6079. DOI: https://doi.org/10.1016/j.jeurceramsoc.2021.05.041.

(29) Thompson, T.; Wolfenstine, J.; Allen, J. L.; Johannes, M.; Huq, A.; David, I. N.; Sakamoto, J. Tetragonal vs. cubic phase stability in Al – free Ta doped Li7La3Zr2O12 (LLZO). *Journal of Materials Chemistry A* **2014**, *2* (33), 13431-13436, 10.1039/C4TA02099E. DOI: 10.1039/C4TA02099E.

(30) Meesala, Y.; Liao, Y.-K.; Jena, A.; Yang, N.-H.; Pang, W. K.; Hu, S.-F.; Chang, H.; Liu, C.-E.; Liao, S.-C.; Chen, J.-M.; et al. An efficient multi-doping strategy to enhance Li-ion conductivity in the garnet-type solid electrolyte Li7La3Zr2O12. *Journal of Materials Chemistry A* **2019**, *7* (14), 8589-8601, 10.1039/C9TA00417C. DOI: 10.1039/C9TA00417C.

(31) Han, X.; Gong, Y.; Fu, K.; He, X.; Hitz, G. T.; Dai, J.; Pearse, A.; Liu, B.; Wang, H.; Rubloff, G.; et al. Negating interfacial impedance in garnet-based solid-state Li metal batteries. *Nature Materials* **2017**, *16* (5), 572-579. DOI: 10.1038/nmat4821.

(32) Chaumont, A.; Wipff, G. M3+ Lanthanide Chloride Complexes in "Neutral" Room Temperature Ionic Liquids: A Theoretical Study. *The Journal of Physical Chemistry B* **2004**, *108* (10), 3311-3319. DOI: 10.1021/jp036229t.

(33) Huggins, R. A. Simple method to determine electronic and ionic components of the conductivity in mixed conductors a review. *Ionics* **2002**, *8* (3), 300-313. DOI: 10.1007/BF02376083.

(34) O.V, S.; R, M. An enhanced interface between garnet solid electrolyte and lithium through multifunctional lithium titanate anode-additive for solid-state lithium batteries. *Journal of Alloys and Compounds* **2023**, *939*, 168774. DOI: https://doi.org/10.1016/j.jallcom.2023.168774.

(35) Nie, K.; Hong, Y.; Qiu, J.; Li, Q.; Yu, X.; Li, H.; Chen, L. Interfaces Between Cathode and Electrolyte in Solid State Lithium Batteries: Challenges and Perspectives. *Front Chem* **2018**, *6*, 616. DOI: 10.3389/fchem.2018.00616 From NLM.

(36) Zahiri, B.; Patra, A.; Kiggins, C.; Yong, A. X. B.; Ertekin, E.; Cook, J. B.; Braun, P. V. Revealing the role of the cathode–electrolyte interface on solid-state batteries. *Nature Materials* **2021**, *20* (10), 1392-1400. DOI: 10.1038/s41563-021-01016-0.

(37) Nie, K.; Hong, Y.; Qiu, J.; Li, Q.; Yu, X.; Li, H.; Chen, L. Interfaces Between Cathode and Electrolyte in Solid State Lithium Batteries: Challenges and Perspectives. *Frontiers in Chemistry* **2018**, *6*, Review. DOI: 10.3389/fchem.2018.00616.

(38) Negi, R. S.; Minnmann, P.; Pan, R.; Ahmed, S.; J. Herzog, M.; Volz, K.; Takata, R.; Schmidt, F.; Janek, J.; Elm, M. T. Stabilizing the Cathode/Electrolyte Interface Using a Dry-Processed Lithium Titanate Coating for All-Solid-State Batteries. *Chemistry of Materials* **2021**, *33* (17), 6713-6723. DOI: 10.1021/acs.chemmater.1c01123.

(39) Glass, A. M.; Nassau, K.; Negran, T. J. Ionic conductivity of quenched alkali niobate and tantalate glasses. *Journal of Applied Physics* **1978**, *49* (9), 4808-4811. DOI: 10.1063/1.325509.

(40) Pervez, S. A.; Kim, G.; Vinayan, B. P.; Cambaz, M. A.; Kuenzel, M.; Hekmatfar, M.; Fichtner, M.; Passerini, S. Overcoming the Interfacial Limitations Imposed by the Solid–Solid Interface in Solid-State Batteries Using Ionic Liquid-Based Interlayers. *Small* **2020**, *16* (14), 2000279. DOI: https://doi.org/10.1002/smll.202000279.

(41) Ke, X.; Wang, Y.; Dai, L.; Yuan, C. Cell failures of all-solid-state lithium metal batteries with inorganic solid electrolytes: Lithium dendrites. *Energy Storage Materials* **2020**, *33*, 309-328. DOI: https://doi.org/10.1016/j.ensm.2020.07.024.

(42) Feng, W.; Dong, X.; Li, P.; Wang, Y.; Xia, Y. Interfacial modification of Li/Garnet electrolyte by a lithiophilic and breathing interlayer. *Journal of Power Sources* **2019**, *419*, 91-98. DOI: https://doi.org/10.1016/j.jpowsour.2019.02.066.

(43) Gao, H.; Yan, S.; Wang, J.; Huang, Y. A.; Wang, P.; Li, Z.; Zou, Z. Towards efficient solar hydrogen production by intercalated carbon nitride photocatalyst. *Physical Chemistry Chemical Physics* **2013**, *15* (41), 18077-18084, 10.1039/C3CP53774A. DOI: 10.1039/C3CP53774A.

(44) Biswas, A.; Kapse, S.; Thapa, R.; Dey, R. S. Oxygen Functionalization-Induced Charging Effect on Boron Active Sites for High-Yield Electrocatalytic NH3 Production. *Nano-Micro Letters* **2022**, *14* (1), 214. DOI: 10.1007/s40820-022-00966-7.

(45) Rais, B.; Ostrowski, E. T.; Canton, A.; Skinner, C. H.; Barison, S.; Fiameni, S.; Koel, B. E. SIMS and HR-XPS characterization of lithiated graphite from the magnetic fusion device RFX-mod. *Applied Surface Science* **2021**, *567*, 150830. DOI: https://doi.org/10.1016/j.apsusc.2021.150830.

(46) Hausbrand, R.; Cherkashinin, G.; Ehrenberg, H.; Gröting, M.; Albe, K.; Hess, C.; Jaegermann, W. Fundamental degradation mechanisms of layered oxide Li-ion battery cathode materials: Methodology, insights and novel approaches. *Materials Science and Engineering: B* **2015**, *192*, 3-25. DOI: https://doi.org/10.1016/j.mseb.2014.11.014.

(47) Kalapsazova, M.; Stoyanova, R.; Zhecheva, E.; Tyuliev, G.; Nihtianova, D. Sodium deficient nickel–manganese oxides as intercalation electrodes in lithium ion batteries. *Journal of Materials Chemistry A* **2014**, *2* (45), 19383-19395, 10.1039/C4TA04094E. DOI: 10.1039/C4TA04094E.

(48) Wu, K.; Hu, N.; Wang, S.; Geng, Z.; Deng, W. Enhancing Performance of LiFePO4 Battery by Using a Novel Gel Composite Polymer Electrolyte. *Batteries* **2023**, *9* (1), 51.

(49) Paronyan, T. M.; Thapa, A. K.; Sherehiy, A.; Jasinski, J. B.; Jangam, J. S. D. Incommensurate Graphene Foam as a High Capacity Lithium Intercalation Anode. *Scientific Reports* **2017**, *7* (1), 39944. DOI: 10.1038/srep39944.

(50) He, M.; Guo, R.; Hobold, G. M.; Gao, H.; Gallant, B. M. The intrinsic behavior of lithium fluoride in solid electrolyte interphases on lithium. *Proceedings of the National Academy of Sciences* **2020**, *117* (1), 73-79. DOI: doi:10.1073/pnas.1911017116.

(51) Zhang, Q.; Ma, J.; Mei, L.; Liu, J.; Li, Z.; Li, J.; Zeng, Z. In situ TEM visualization of LiF nanosheet formation on the cathode-electrolyte interphase (CEI) in liquid-electrolyte lithium-ion batteries. *Matter* **2022**, *5* (4), 1235-1250. DOI: https://doi.org/10.1016/j.matt.2022.01.015.

(52) Wagner, N. P.; Asheim, K.; Vullum-Bruer, F.; Svensson, A. M. Performance and failure analysis of full cell lithium ion battery with LiNi0.8Co0.15Al0.05O2 and silicon electrodes. *Journal of Power Sources* **2019**, *437*, 226884. DOI: https://doi.org/10.1016/j.jpowsour.2019.226884.

(53) Dose, W. M.; Maroni, V. A.; Piernas-Muñoz, M. J.; Trask, S. E.; Bloom, I.; Johnson, C. S. Assessment of Li-Inventory in Cycled Si-Graphite Anodes Using LiFePO4 as a Diagnostic

Cathode. *Journal of The Electrochemical Society* **2018**, *165* (10), A2389. DOI: 10.1149/2.1271810jes.